Chapter 12
CA Modeling of Ant-Traffic on Trails

Debashish Chowdhury, Katsuhiro Nishinari, and Andreas Schadschneider

12.1 Introduction

There has been significant progress in modelling complex systems by using cellular automata (CA) [1, 2]; such complex systems include, for example vehicular traffic [3] and biological systems [4, 5]. In most cases, particle-hopping CA models have been used to study the spatio-temporal organization in systems of interacting particles driven far from equilibrium [2, 3]. In traffic systems, vehicles are represented by particles while their mutual influence is captured by the inter-particle interactions. Generically, these inter-particle interactions tend to hinder their motions which leads a monotonic decrease of the average speed as function of the particle density [6, 7].

Physicists, applied mathematicians, statisticians and traffic engineers have developed a variety of models which can reproduce the empirically observed properties of vehicular traffic rather accurately [3, 8, 9]. Here we describe an extension of a particularly successful approach based on CA to a seemingly different problem, namely the traffic-like collective movements of ants on trails [10, 11] (see Fig. 12.1). Following this approach, we develop a model which predicts a counter-intuitive result [6]. More specifically, the model predicts a non-monotonic variation of the average speed of ants with their density on the trail. Some of the predictions of this model of ant-traffic have been tested in recent empirical investigation [12]. Most of this chapter is a review of our earlier papers published elsewhere. However, we present this critical overview from our current perspective in the light of the developments over the last few years.

The similarity between ant traffic and vehicular traffic on highways has also been noted by biologists. Burd et al. [13] were the first to measure the average speed of ants on a trail as a function of density. In traffic engineering this corresponds to the so-called *fundamental diagram* which is – as indicated by the name – the most important characteristics of traffic dynamics.

D. Chowdhury (✉)
Department of Physics, Indian Institute of Technology, Kanpur 208016, India
e-mail: debch@iitk.ac.in

A.G. Hoekstra et al. (eds.), *Simulating Complex Systems by Cellular Automata*,
Understanding Complex Systems, DOI 10.1007/978-3-642-12203-3_12,

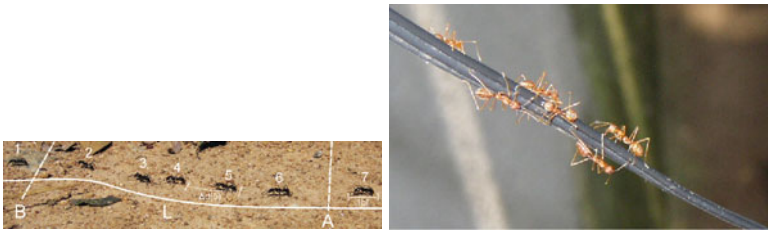

Fig. 12.1 Examples for ant trails

This chapter is organized as follows: First, in Sect. 12.2, we define the basic model for uni-directional traffic on an existing single-lane ant trail. In Sect. 12.4, we extend this model to capture bi-directional traffic on a two-lane ant-trail. We discuss a model of bi-directional traffic on a single-lane ant-trail in Sect. 12.5. Then, in Sect. 12.6 we report results from a recent empirical study and compare with the predictions of the model. Finally, in Sect. 12.7 we summarize the main conclusions.

12.2 A Model of Unidirectional Traffic on a Single-Lane Ant Trail

The models which will be described in the following assume the existence of a fully developed ant trail on which a steady flow takes place. The formation of the trail itself is a problem of self organization which has been studied quite extensively in the past (see e.g. [14] for an overview).

Let us first define the ant trail model (ATM) which is a simple model for a unidirectional collective movement of ants on a pre-existing single-lane ant trail. The ants communicate with each other by dropping a chemical (generically called *pheromone*) on the substrate as they move forward [15, 16]. The pheromone sticks to the substrate long enough for the other following ants to pick up the chemical signal and follow the trail. This mechanism is captured in the ATM by extending the *asymmetric simple exclusion process (ASEP)* [17–20], the simplest and most studied model for driven diffusive systems.

ASEP can be interpreted as a cellular automaton model. It describes the directed motion of particles on a discrete one-dimensional lattice of sites each of which represents the center of a cell. Each cell can be occupied by at most one particle at a time. Identifying the particles in the ASEP with ants we need to incorporate pheromone-mediated interactions among the ants. This leads to an ASEP-like model where the hopping probability of a particle depends on the state of the target cell (see Fig. 12.2).

The cells are labelled by the index i ($i = 1, 2, \ldots, L$) where L is the length of the lattice. One associates two binary variables S_i and σ_i with each site i where S_i takes the value 0 or 1 depending on whether the cell is empty or occupied by an ant. Similarly, $\sigma_i = 1$ if the cell i contains pheromone; otherwise, $\sigma_i = 0$. The

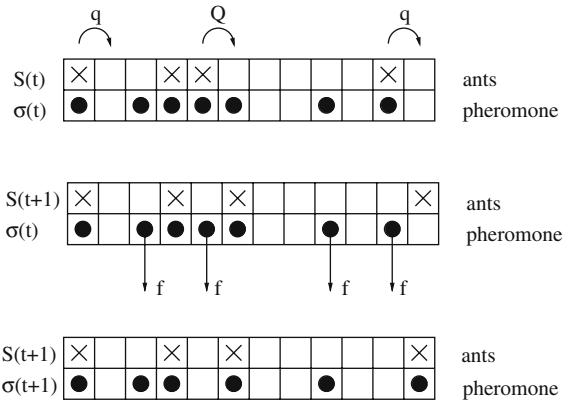

Fig. 12.2 Illustration of the update procedure in the ATM. *Top*: Configuration at time t, i.e. *before* stage I of the update. The non-vanishing hopping probabilities of the ants are shown explicitly. *Middle*: Configuration *after* one possible realisation of *stage I*. Also indicated are the pheromones that may evaporate in stage II of the update scheme. *Bottom*: Configuration *after* one possible realization of *stage II*. Two pheromones have evaporated and one pheromone has been created due to the motion of an ant

instantaneous state (i.e., the configuration) of the system at any time is specified completely by the set $(\{S\}, \{\sigma\})$.

Since a unidirectional motion is assumed, ants do not move backward. Their forward-hopping probability is higher if there is pheromone ahead of it. The state of the system is updated at each time step in *two stages*. In stage I ants are allowed to move. Here the subset $\{S(t+1)\}$ at the time step $t+1$ is obtained using the full information $(\{S(t)\}, \{\sigma(t)\})$ at time t. Stage II corresponds to the evaporation of pheromone. Here only the subset $\{\sigma(t)\}$ is updated so that at the end of stage II the new configuration $(\{S(t+1)\}, \{\sigma(t+1)\})$ at time $t+1$ is obtained. In each stage the dynamical rules are applied *in parallel* to all ants and pheromones, respectively.

Stage I: Motion of ants

An ant in cell i that has an empty cell in front of it, i.e., $S_i(t) = 1$ and $S_{i+1}(t) = 0$, hops forward with

$$\text{probability} = \begin{cases} Q & \text{if } \sigma_{i+1}(t) = 1, \\ q & \text{if } \sigma_{i+1}(t) = 0, \end{cases} \tag{12.1}$$

where, to be consistent with real ant-trails, we assume $q < Q$.

Stage II: Evaporation of pheromones

At each cell i occupied by an ant after stage I a pheromone will be created:

$$\sigma_i(t+1) = 1 \quad \text{if} \quad S_i(t+1) = 1. \tag{12.2}$$

In addition, any "free" pheromone at a site i, which is not occupied by an ant, will evaporate with the probability f per unit time, i.e., if $S_i(t+1) = 0$, $\sigma_i(t) = 1$, then

$$\sigma_i(t+1) = \begin{cases} 0 & \text{with probability } f, \\ 1 & \text{with probability } 1-f. \end{cases} \tag{12.3}$$

The dynamics conserves the number N of ants, but not the number of pheromones. We first discuss the case of periodic boundary conditions which simplifies the theoretical analysis. An extension to the case of the open boundary conditions [21], which is more relevant for the application to real trails, is briefly discussed later.

Formally, the rules can be written in compact form as the coupled equations

$$\begin{aligned} S_j(t+1) = S_j(t) &+ \min(\eta_{j-1}(t), S_{j-1}(t), 1 - S_j(t)) \\ &- \min(\eta_j(t), S_j(t), 1 - S_{j+1}(t)), \end{aligned} \tag{12.4}$$

$$\sigma_j(t+1) = \max(S_j(t+1), \min(\sigma_j(t), \xi_j(t))), \tag{12.5}$$

where ξ and η are stochastic variables defined by

$$\xi_j(t) = \begin{cases} 0 & \text{with probability } f \\ 1 & \text{with probability } 1-f \end{cases}, \tag{12.6}$$

$$\eta_j(t) = \begin{cases} 1 & \text{with probability } p = q + (Q-q)\sigma_{j+1}(t) \\ 0 & \text{with probability } 1-p \end{cases}. \tag{12.7}$$

In the limits $f = 0$ and $f = 1$ the model reduces to the ASEP. For $f = 0$ a pheromone, once created, will never evaporate. So in the stationary state all cells are occupied by pheromone and the ants will always move with rate Q. For $f = 1$, on the other hand, each pheromone will evaporate immediately. Therefore, in the stationary state, the ants will always move with rate q.

This is reflected in Eqs. (12.4) and (12.5) which reduce to the ASEP if we choose p as a constant, i.e., p does not depend on σ. If we further consider the deterministic limit $p = 1$, then this model reduces to the Burgers CA [22], which is also known as an exactly solvable CA. It should also be mentioned that the ATM is closely related to the bus-route models [23, 24].

12.2.1 Computer Simulation Results

The ASEP [17–20] with parallel updating has been used often as an extremely simple model of vehicular traffic on single-lane highways. The most important quantity of interest in the context of flow properties of the traffic models is the *fundamental diagram*, i.e., the flow-versus-density relation, where flow J is the product of the density ρ and the average speed v. It is especially relevant if one wants to compare the properties of ant traffic with those of vehicular traffic. The flow (or current) J and the average speed v of vehicles are related by the *hydrodynamic relation*

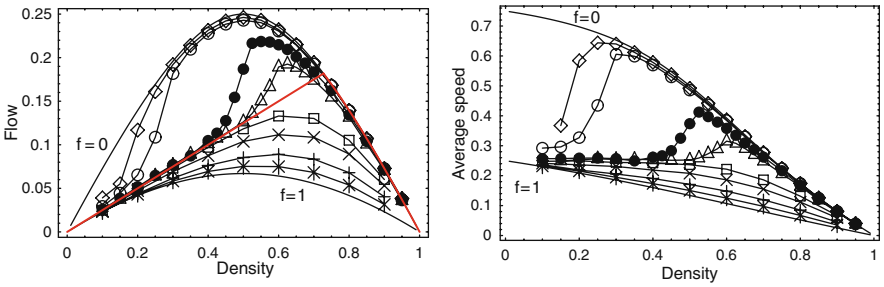

Fig. 12.3 The average flow (*left*) and speed (*right*) of the ants, extracted from computer simulation data, are plotted against their densities for the parameters $Q = 0.75, q = 0.25, L = 500$ and evaporation probabilities $f = 0.0005(\diamond)$, $0.001(\circ)$, $0.005(\bullet)$, $0.01(\triangle)$, $0.05(\square)$, $0.10(\times)$, $0.25(+)$, $0.50(*)$. The *lines* connecting these data points merely serve as the guide to the eye. The cases $f = 0$ and $f = 1$ are also displayed, which are identical to the ASEP corresponding to the effective hopping probabilities Q and q, respectively. The analytical curve corresponds to $f \to 0$ in the thermodynamic limit, which is discussed in Sect. 12.2.2 is also depicted (the thick *red curve* without ornaments)

$J = \rho v$ and, therefore, either of the functions $J(\rho)$ and $v(\rho)$ can be used to express the effects of interactions of the ants on the flow.

Fundamental diagrams of the ATM obtained by computer simulations are shown in Fig. 12.3. In the ASEP the flow remains invariant under the interchange of ρ and $1 - \rho 0$; this particle-hole symmetry leads to a fundamental diagram that is symmetrical about $\rho = \frac{1}{2}$. In the ATM, a particle-hole symmetry is only observed in the special cases $f = 0$ and $f = 1$ where it reduces to the ASEP.

However, the most surprising observation is that over a range of small values of f, the fundamental diagram exhibits an anomalous behaviour. Unlike common vehicular traffic, v is not a monotonically decreasing function of the density ρ (Fig. 12.3). Instead, a relatively sharp crossover can be observed where the speed *increases* with the density. In the usual form $J(\rho)$ of the fundamental diagram this transition leads to the existence of an inflection point (Fig. 12.3).

By a detailed analysis of the spatio-temporal organizations in the steady-state, we were able to distinguish three different regimes of density. At low densities a loosely assembled cluster is formed (Fig. 12.4) that propagates with the probability q. These clusters are rather different from jam clusters encountered in highway traffic which have a density close to the maximal density and move in a direction opposite to the direction of motion of the particles (cars). In contrast, a *loose cluster* has a typical density $\rho_{\ell c}$ which is larger than the average density ρ, but smaller than the maximal density $\rho = 1$, i.e. $\rho < \rho_{\ell c} < 1$. It moves in the same direction as the ants. The leading ant in the cluster which typically hops with probability q will determine the velocity of the cluster.

In the intermediate density regime, the leading ant occasionally hops with probability Q instead of q, because sometimes it feels the pheromone dropped by the last ant in the cluster. This arises from the fact that, because of the periodic boundary conditions, the gap size between the last and leading ant becomes shorter as the

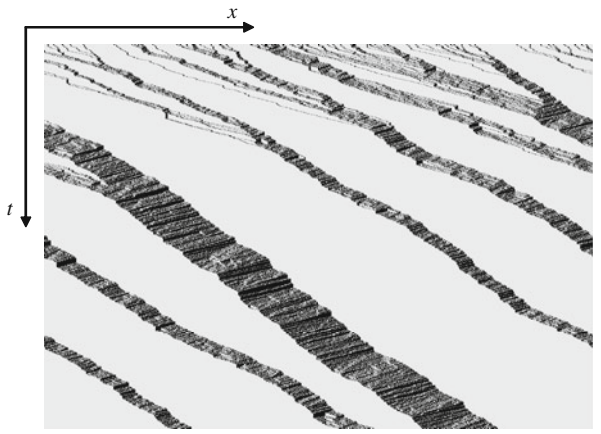

Fig. 12.4 Spatial-temporal behaviour of loose clusters in the low density case ($\rho = 0.16$). Parameters are $Q = 0.75, q = 0.25, f = 0.005$). Loose clusters emerge from the random initial configuration and will eventually merge into one big loose cluster after sufficiently long time

cluster becomes larger, so that the leading ant is likely to find the pheromone in front of it. This increase of the average speed in the intermediate-density region (Fig. 12.3) leads to the anomalous fundamental diagram.

Finally, at high densities, the mutual hindrance against the movements of the ants dominates the flow behaviour. This leads to a homogeneous state similar to that of the ASEP. In this regime loose clusters no longer exist and ants are uniformly distributed after a long time. Thus homogeneous mean-field theories can account for the qualitative features of the fundamental diagram only in this regime.

12.2.2 Analytical Results

So far, an exact solution for the stationary state of the ATM has not been achieved. However, it is possible to describe the dynamics rather well using approximate analytical theories.

First, mean-field type approaches have been suggested [6, 7]. However, homogeneous mean-field theories fail in the intermediate density regime. Here the loose cluster dominates the dynamics which can not be described properly by the mean-field theories which assume a uniform distribution of the ants.

12.2.2.1 ZRP and ATM

A better theoretical treatment of ATM can be formulated by realizing [7, 21] that the ATM is closely related to the *zero-range process* (*ZRP*), which is one of the exactly solvable models of interacting Markov processes [25–27]. The ZRP consists of the moving particles of the exclusion process, but in contrast, these particles do

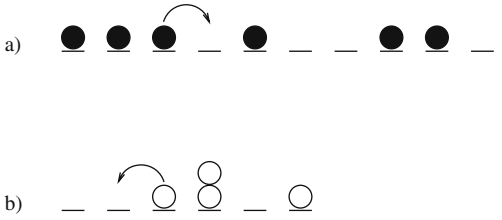

Fig. 12.5 Illustration of the mapping between (**a**) the ASEP and (**b**) a ZRP. Particles of the ASEP become lattice sites in the ZRP. The number of particles at a site in the ZRP corresponds to the headway in ASEP picture. Particles in the ZRP representation move in the opposite direction than in the ASEP representation

not obey an exclusion principle. Therefore each lattice site can be occupied by an arbitrary number of particles. A distinct characteristic of the ZRP is the special form of the transition probabilities. The hopping probability of a particle to its nearest neighbour site depends only on the number of the starting site, not that at the target site.

The ASEP can be interpreted as a special ZRP where the particles in the ASEP are identified with the sites in the ZRP [26, 27]. The number of particles present at a site j is then given by the number of empty cells in front of particle j in the ASEP, also known as *headway* in traffic engineering. This mapping is shown in Fig. 12.5.

In ATM representation, the hopping probability u can be expressed as

$$u = q(1 - g) + Qg, \tag{12.8}$$

where g is the probability that there is a surviving pheromone on the first site of a gap. Assume that the gap size is x and the average velocity of ants is v. Since $g(t + 1) = (1 - f)g(t)$ holds at each time step, we obtain $g(x) = (1 - f)^{x/v}$ after iterating it by x/v times, which is the time interval of between the passage of successive ants through any arbitrary site. Note that in this argument we have implicitly used a mean field approximation: that the ants move with the mean velocity v maintaining equal spacing x. Thus, in the ATM the hopping probability u is related to gaps x by [6]

$$u(x) = q + (Q - q)(1 - f)^{x/v}. \tag{12.9}$$

Using the formal mapping between the ZRP and ASEP we conclude that the steady state of the ATM can be well described by that of the ZRP with parallel dynamics. This allows one to translate the known exact results of the stationary state of the ZRP to the ATM case.

The average velocity v of ants is calculated by

$$v = \sum_{x=1}^{L-N} u(x)\, p(x) \tag{12.10}$$

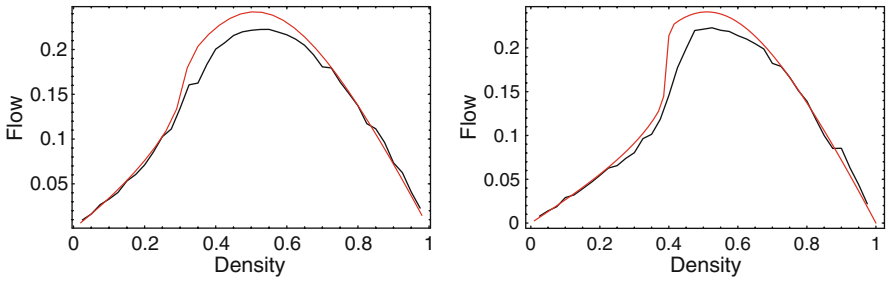

Fig. 12.6 The fundamental diagram of the ATM for system sizes $L = 100$ (*left*) and $L = 200$ (*right*). The dynamical parameters are $Q = 0.75$, $q = 0.25$, $f = 0.005$. The smooth *red curve* has been obtained from the ZRP description while the zigzaged *black one* is the numerical data

since the number of particles in the ZRP picture is $L - N$. $p(x)$ is the probability of finding a gap of size x, which is given by

$$p(x) = h(x)\frac{Z(L - x - 1, N - 1)}{Z(L, N)}, \tag{12.11}$$

where $Z(L, N)$ is usually called *partition function* since it appears as normalization factor in the probability distribution of headway configurations [21].

Since the ATM is formulated with parallel update, the form of $h(x)$, as calculated in (12.11), is given by [28]

$$h(x) = \begin{cases} 1 - u(1) & \text{for} \quad x = 0 \\ \dfrac{1 - u(1)}{1 - u(x)} \displaystyle\prod_{y=1}^{x} \dfrac{1 - u(y)}{u(y)} & \text{for} \quad x > 0 \end{cases}. \tag{12.12}$$

The partition function Z is obtained by the recurrence relation

$$Z(L, N) = \sum_{x=0}^{L-N} Z(L - x - 1, N - 1)h(x), \tag{12.13}$$

with $Z(x, 1) = h(x - 1)$ and $Z(x, x) = h(0)$, which is easily obtained by (12.11) with the normalization $\sum p(x) = 1$.

The fundamental diagram of the ATM can be derived by using (12.10) with changing ρ from 0 to 1. The velocity v in (12.9) can be set to $v = q$, which is known to be a good approximation for v [23]. Strictly speaking, v should be determined self-consistently by (12.9) and (12.10). Figure 12.6 shows results for $L = 100$ and $L = 200$. The good agreement with the simulation data confirms that the ZRP provides an accurate description of the steady state of the ATM.

12.2.2.2 Thermodynamic Limit of ATM

Next we discuss the thermodynamic limit of the ATM, that is, the case $L \to \infty$ with $\rho = N/L$ fixed. From Fig. 12.3 we see that the curve shows sharp increase near the density region $0.4 < \rho < 0.5$, and the tendency is expected to be even stronger with the increase of L. This indicates the possibility of a phase transition in the thermodynamic limit. The mapping to the ZRP is exploited to explore this possibility in an analytic way by determining the behaviour of $Z(L, N)$ in the thermodynamic limit. First $Z(L, N)$ is represented as an integral which can be evaluated by the saddle point method [28]. A central role is played by the generating function $G(s)$ of h defined by

$$G(s) = \sum_{x=0}^{\infty} h(x) s^x . \tag{12.14}$$

It can be shown [21] that G converges in the range

$$0 < z < z_c = \frac{q}{1-q} , \tag{12.15}$$

where z is defined by

$$\frac{1}{\rho} - 1 = z \frac{\partial \ln G(z)}{\partial z} . \tag{12.16}$$

In the case $f > 0$, $G(z_c)$ diverges which implies that there is no phase transition. This is because from (12.16), we have $\rho = 1$ when $z = 0$, and $\rho = 0$ at $z = z_c$ if $G(z_c)$ diverges. Thus, in the entire density region $0 \le \rho \le 1$ there is no singularity in G and, hence, no phase transition in the ATM.

The situation drastically changes in the limit $f \to 0$ since then $G(z_c)$ becomes finite. Thus there is a phase transition in the case $f = 0$ at a critical density

$$\rho_c = \frac{Q-q}{Q-q^2} \tag{12.17}$$

obtained from (12.16). The corresponding average velocity at $z = z_c$ is found as

$$v_c = q . \tag{12.18}$$

It should be noted [7] that (12.17) is also obtained by the intersection point of the line $J = v_c \rho$ and the ASEP curve [3]

$$J = \frac{1}{2} \left(1 - \sqrt{1 - 4Q\rho(1-\rho)} \right) \tag{12.19}$$

in the flow-density diagram. Note that the limits $L \to \infty$ and $f \to 0$ do not commute [23]. If one takes $f \to 0$ before $L \to \infty$, then the flow is given by the ASEP result (12.19). This order is relevant for the case of numerical simulations. On the other hand, if $f \to 0$ is taken after $L \to \infty$, one obtains the thick curve in Fig. 12.3 and the anomalous variation of the average velocity with density disappears.

12.2.2.3 Open Boundary Conditions

So far we have considered the ATM with only periodic boundary conditions. However, for ant trails the open boundary conditions are more realistic.

Suppose α and β denote the probabilities of incoming and outgoing particles at the open boundaries per unit time. The phase diagram of the ASEP in the $\alpha-\beta$-plane is well understood [19]. Here we summarize the effects of varying the pheromone evaporation probability f on this phase diagram.

Just as in the case of the ASEP, for all f one finds three different phases, namely, the *high-density phase*, the *low-density phase* and the *maximal current phase* (see Fig. 12.7). In the low-density phase the current is limited by the low input probability α and is therefore independent of β. In contrast, in the high-density phase the particle removal at the end of the chain is the current-limiting factor and thus the current is independent of α. Finally, in the maximal current phase the current is limited by the bulk transport capacity. Here J is independent of both α and β.

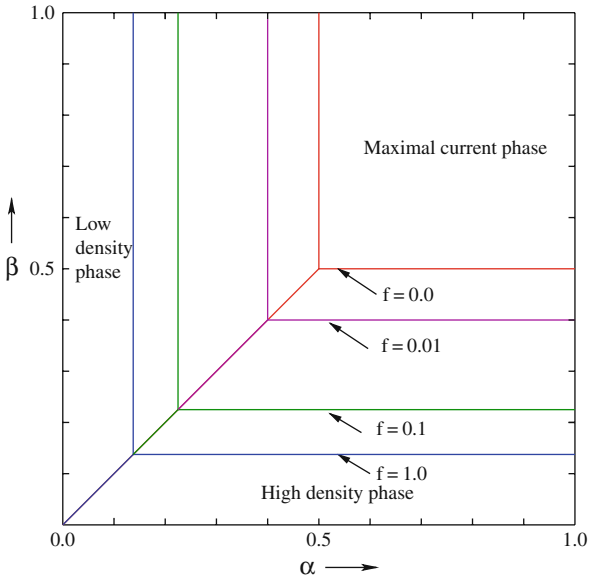

Fig. 12.7 The phase diagram of the ATM with open boundary conditions in the $\alpha - \beta$-plane for several values of the pheromone evaporation probability f ($0 \leq f \leq 1$). The values of the hopping parameters are $Q = 0.75$, $q = 0.25$

The location $\alpha_c(f)$ and $\beta_c(f)$ of the phase transition lines in the ATM depends on the evaporation rate f. A more quantitative understanding of the phase diagram [21] can be obtained by extending the domain wall theory [29, 30] developed for driven diffusive systems with open boundaries to the ATM case. Many properties of the open system can be extracted from those of the corresponding system under periodic boundary conditions.

12.3 The Multi Robots Implementation

An alternative to the cellular automaton computer simulation is the implementation of the ant trail model as a robotic system [31]. Here social insects are used as a source of inspiration. Aggregation patterns for example are the basis for collective action or collaboration.

12.3.1 Experimental Setup

Here we will focus on the unidirectional case where all robots move on a circular track. The ant-pheromone interaction is incorporated by a virtual pheromone system (V-DEAR). A virtual pheromone field is projected onto the circular track and perceived and modified by the robots (see Fig. 12.8). The concentration of pheromones $p(x,t) \in [0, P_0]$ is indicated by the color and brightness of the projected field. Depending on the concentration, two velocities can be assumed by the robots:

$$v(x) = \begin{cases} V_Q & \text{for } p(x,t) \geq p_{\text{th}} \\ V_q & \text{for } p(x,t) < p_{\text{th}} \end{cases} \tag{12.20}$$

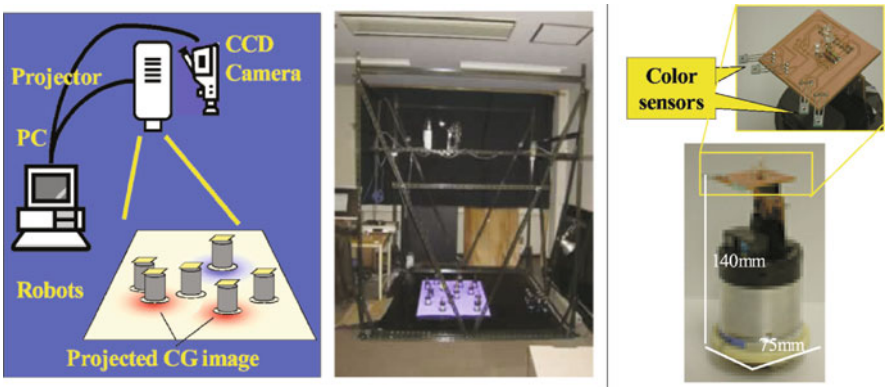

Fig. 12.8 Experimental setup for the multiple robots experiment: Robots serving as ants move on a circular track (*left*). Their positions are traced by a CCD camera. An artificial pheromone field is projected on the track. The robots (*right*) are equipped with sensors to detect its color and brightness

Table 12.1 The parameters for the experimental setup are shown here. For a better comparison with cellular automaton models lengths are additionally given in units of the body-length (bl) of one single robot. At $\rho = 1$ the circular track is occupied by 22 robots. The dimensionless pheromone concentration ranges from 0 to 250

V_Q (cm/s)	V_q (cm/s)	L (robot)	p_{th}	P_0
7 (0.94 bl/sec)	1.4 (0.19 bl/sec)	22 (22 bl)	127	250

Unlike in the ATM, the gradient of the pheromone concentration does not lead to a corresponding gradient of velocity depending on the distance to the preceding ant. Therefore only the difference to the threshold value p_{th} is of importance.

The dynamics of the virtual pheromone field is very much the same as in the ATM. The positions of the robots are detected by a CCD camera and the pheromone field is modified accordingly. A robot occupying site x leads to the maximal pheromone concentration P_0 at that site. An unoccupied site is described by a decaying pheromone concentration:

$$p(x,t) = \begin{cases} P_0 & \text{if } x \text{ is occupied} \\ P_0 \exp(-\lambda_f t) & \text{else} \end{cases} . \tag{12.21}$$

For $\lambda_f = 0$ the pheromone concentration always exceeds $p_{\text{th}} < P_0$ once a site has been occupied by a robot leading to V_Q. Unlike in the undirectional model $\lambda_f = 1$ does not lead to an instantaneous evaporation. For the corresponding case $\lambda_f \longrightarrow \infty$ or at least $\lambda_f \gg 1$ is needed.

For the experiment two different intrinsic velocities V_q and V_Q were used (see Table 12.1). The threshold value for the pheromone concentration p_{th} was chosen such that the pheromone trace is of finite length. For our system this means that the pheromone trace following each robot reaches a concentration $p < p_{\text{th}}$ before it assumes $p = P_0$ due to the presence of a succeeding robot. Blocking is incorporated in the same way as in the unidirectional ATM. A robot which has caught up with the preceding one has to stop for one second. Due to this mechanism no overtaking is possible. In analogy with the ATM, this mechanism ensures the simple exclusion principle.

12.3.2 Observations

The observed behaviour in the experimental setup qualitatively agrees with that of the ATM. Initially the robots are distributed homogeneously on the circle (Fig. 12.9). Each robot is followed by a trace of light which is the equivalent of the pheromone trace. The trace is of finite length which is set by the evaporation constant λ_f. Although the robots in principle behave deterministically, fluctuations are induced by various perturbations, e.g., noise arising from friction. As a result the distances between two robots might accidently reduce in such a way that the succeeding robot is affected by the pheromone trace of the preceding one. Generally some robots

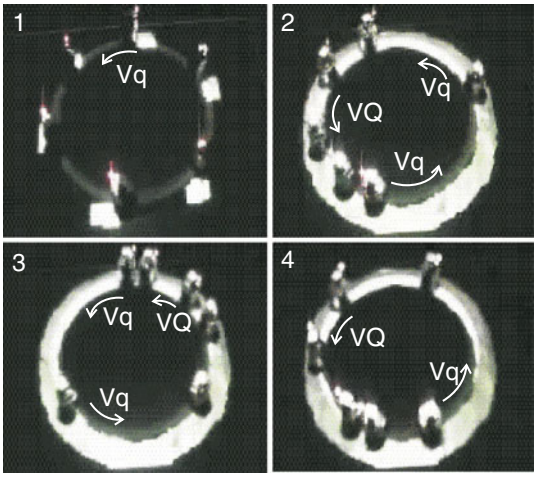

Fig. 12.9 Platoon formation in the robot experiment: (1) In the initial state the robots are placed homogeneously on the circular track. (2) Each robot is followed by a pheromone trace of finite length. Robots perceiving this trace move with V_Q and with $V_q < V_Q$ otherwise. As a result a platoon is formed as robots tend to collect behind a slow robot moving with V_q. (3) Robots within a platoon catch up with V_Q. (4) At later times only one platoon moving with V_q is left

will move with V_Q whereas others move with V_q. In the final stage a stable platoon moving with a velocity V_q is formed (Fig. 12.9).

Flow is measured directly by the number of robots passing a fixed point on the track in a certain time interval. From this the average velocity is calculated using the hydrodynamic relation. For $f = 0$ the behaviour of the system is roughly identical to that of the ASEP (Fig. 12.10). At low densities, flow increases almost linearly. For densities larger than $\rho = \frac{1}{2}$ flow finally decreases. Overall this shows that effects arising from mutual blocking are also present in the robot experiment. Unlike in the ATM, $\lambda_f = 1$ does not correspond to an instantaneous evaporation of the pheromones. Therefore the ASEP-case is not recovered in this limit and a nearly constant average velocity is observed (Fig. 12.10). Furthermore, similar to the ATM, non-monotonic behaviour of the velocity is observed for small values of λ_f.

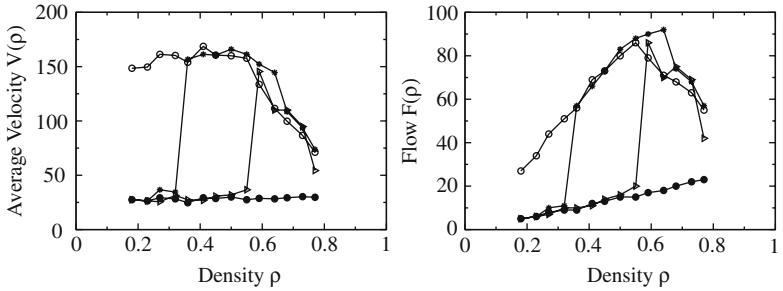

Fig. 12.10 Fundamental diagrams for the robot implementation of the ATM: $V_Q = 7\,\mathrm{cm/s}$, $V_q = 1.4\,\mathrm{cm/s}$ and $\lambda_f = 0(\circ)$, $0.03(*)$, $0.05(\triangleright)$, $1(\bullet)$. For $\lambda_f = 0.03$ and $\lambda_f = 0.05$ the same non-monotonic behaviour as for the computer simulation of the ATM is observed in the density-dependence of the average velocity (left)

12.4 A model of Bidirectional Traffic on a Two-Lane Ant Trail

Real ant trails are often not unidirectional. Instead the trail is shared by ants moving in opposite directions. Therefore an extension of the ATM as described in Sect. 12.2.1 to bidirectional ant traffic is required. We will discuss two different approaches. In this section a two-lane model is introduced with separate lanes for the opposite directions. In Sect. 12.5 a simpler single-lane model is discussed where ants moving in opposite direction share the same lane.

12.4.1 Extensions of the Uni-Directional Model

In this model of bidirectional ant traffic [32] the trail consists of *two* lanes of cells (see Fig. 12.11). These two lanes need not be physically separate rigid lanes in real space; these are, however, convenient for describing the movements of ants in two opposite directions. In the initial configuration, under periodic boundary conditions, a randomly selected subset of the ants move in the clockwise direction in one lane while the others move counterclockwise in the other lane. However, ants are allowed neither to take U-turn [33] nor to change lane. Thus, the ratio of the populations of clockwise-moving and anti-clockwise moving ants remains unchanged as the system evolves with time. All results discussed in the following correspond to the *symmetric* case where equal number of ants move in the two directions. Therefore, the average flux of outbound and nestbound ants are identical.

The rules governing the dropping and evaporation of pheromone in the model of bidirectional ant traffic are identical to those in the model of uni-directional traffic. The *common* pheromone trail is created and reinforced by both the outbound and nestbound ants. The probabilities of forward movement of the ants in the model of bidirectional ant traffic are also natural extensions of the similar situations in the unidirectional traffic. When an ant (in either of the two lanes) *does not* face any other ant approaching it from the opposite direction the likelihood of its forward movement onto the ant-free cell immediately in front of it is Q or q, respectively, depending on whether or not it finds pheromone ahead. Finally, if an ant finds another oncoming ant just in front of it, as shown in Fig. 12.11, it moves forward onto the next cell with probability K.

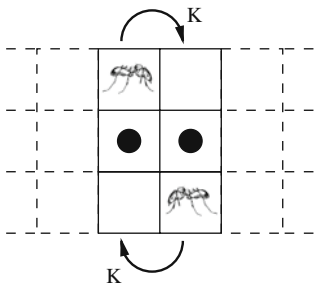

Fig. 12.11 A typical head-on encounter of two oppositely moving ants in the model of *bidirectional* ant traffic

Since ants do not segregate in perfectly well defined lanes, head-on encounters of oppositely moving individuals occur quite often although the frequency of such encounters and the lane discipline varies from one species of ants to another. In reality, two ants approaching each other feel the hindrance, turn by a small angle to avoid head-on collision [34] and, eventually, pass each other. At first sight, it may appear that the ants in the model follow perfect lane discipline. However, that is not true. In the model, the violation of lane discipline and head-on encounters of oppositely moving ants is captured, effectively, in an indirect manner by assuming $K < Q$. But, a left-moving (right-moving) ant *cannot* overtake another left-moving (right-moving) ant immediately in front of it in the same lane. Even in the special limit $K = Q$ the traffic dynamics on two lanes would remain coupled because the pheromone dropped by the outbound ants also influence the nestbound ants and vice versa.

Since for realistic model one has $q < Q$ and $K < Q$, this leaves two interesting parameter regions, namely $q < K < Q$ and $K < q < Q$.

12.4.1.1 Results and Physical Interpretations

The variations of flux with density of ants, for a set of biologically relevant values of the parameters, are shown in Figs. 12.12a and 12.13a; the corresponding average speeds are plotted against density in Figs. 12.12b and 12.13b, respectively. In the Fig. 12.12, the non-monotonic variation of the average speed with density gives rise to the unusual shape of the flux-versus-density diagram over a range of values of f. This feature of the model of bidirectional traffic is similar to that of the unidirectional ant traffic.

An additional feature of the density-dependence of the flux in the bidirectional ant traffic model is the occurrence of a plateau region. This plateau is more pronounced in Fig. 12.13a than in Fig. 12.12a. Such plateaus in the flux-versus-density diagram have been observed earlier [35, 36] in models related to vehicular traffic where randomly placed bottlenecks slow down the traffic in certain locations along

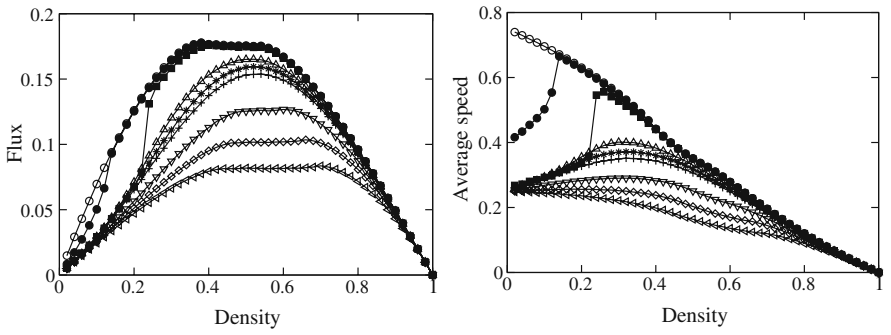

Fig. 12.12 Typical fundamental diagrams for the bidirectional 2-lane model in the case $q < K < Q$. The parameters are $Q = 0.75$, $q = 0.25$ and $K = 0.5$. The symbols ○, ●, ■, △, ∗, +, ▽, ◇ and ◁ correspond, respectively, to $f = 0, 0.0005, 0.005, 0.05, 0.075, 0.10, 0.25, 0.5$ and 1

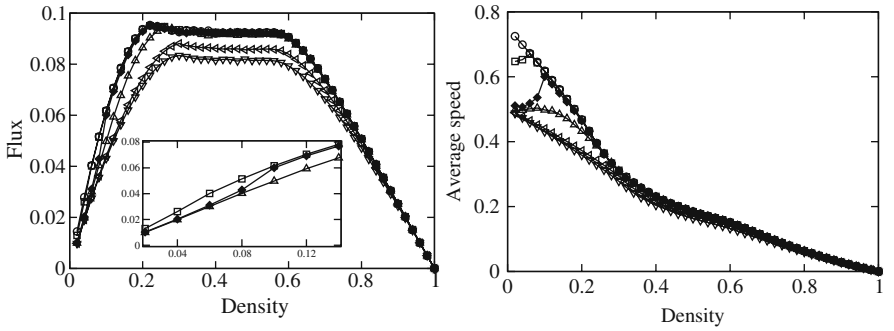

Fig. 12.13 Typical fundamental diagrams for the bidirectional 2-lane model in the case $K < q < Q$. The parameters are $Q = 0.75, q = 0.50$ and $K = 0.25$ The symbols $\circ$, $\square$, $\blacklozenge$, $\triangle$, $\triangleleft$ and $\triangledown$ correspond, respectively, to $f = 0, 0.0005, 0.005, 0.05, 0.5$ and 1. The *inset* in (**a**) is a magnified re-plot of the same data to emphasize the fact that the unusual trend of variation of flux with density in this case is similar to that observed in unidirectional model

the route. Note that in Fig. 12.12a the plateaus appear only in the two limits $f \to 0$ and $f \to 1$ but not for an intermediate range of values of f. In the limit $f \to 0$, most often the likelihood of the forward movement of the ants is $Q = 0.75$ whereas they are forced to move with a smaller probability $K = 0.5$ at those locations where they face another ant immediately in front approaching from the opposite direction (like the situations depicted in Fig. 12.11). Thus, such encounters of oppositely moving ants have the same effect on ant traffic as bottlenecks on vehicular traffic.

But why do the plateaus re-appear in the Fig. 12.12a also in the limit $f \to 1$? At sufficiently high densities, oppositely moving ants facing each other move with probability $K = 0.5$ rather than $q = 0.25$. In this case, locations where the ants have to move with the lower probability q will be, effectively bottlenecks and hence the re-appearance of the plateau. As f approaches unity there will be larger number of such locations and, hence, the wider will be the plateau. This is consistent with our observation in Fig. 12.12a.

12.5 A Model of Bidirectional Traffic on a Single-Lane Ant Trail

In the following we discuss a model, known as *PRL model* [37], where oppositely moving ants share the same trail.

In this model the right-moving (left-moving) particles, represented by R (L), are never allowed to move towards left (right); these two groups of particles are the analogs of the outbound and nest-bound ants in a *bidirectional* traffic on the same trail. Thus, no U-turn is allowed. In addition to the ASEP-like hopping of the particles onto the neighboring vacant sites in the respective directions of motion, the R and L particles on nearest-neighbour sites and facing each other are allowed to exchange their positions, i.e., the transition $RL \stackrel{K}{\to} LR$ takes place, with the probability K. This might be considered as a minimal model for the motion of ants on

a hanging cable as shown in Fig. 12.1. When a outbound ant and a nest-bound ant face each other on the upper side of the cable, they slow down and, eventually, pass each other after one of them, at least temporarily, switches over to the lower side of the cable. Similar observations have been made for normal ant-trails where ants pass each other after turning by a small angle to avoid head-on collision [34, 38]. In our model, as commonly observed in most real ant trails, none of the ants is allowed to overtake another moving in the same direction.

One then introduces a third species of particles, labelled by P, corresponding to the pheromone. The P particles are deposited on the lattice by the R and L particles when the latter hop out of a site; an existing P particle at a site disappears when a R or L particle arrives at the same location. The P particles cannot hop but can evaporate, with a probability f per unit time. None of the lattice sites can accomodate more than one particle at a time.

The state of the system is updated in a random-sequential manner. Using periodic boundary conditions, the densities of the R and the L particles are conserved. In contrast, the density of the P particles is a non-conserved variable. The distinct initial states and the corresponding final states for pairs of nearest-neighbor sites are shown in Fig. 12.14 together with the respective transition probabilties.

Suppose N_+ and $N_- = N - N_+$ are the total numbers of R and L particles, respectively. For a system of length L the corresponding densities are $\rho_\pm = N_\pm/L$ with the total density $\rho = \rho_+ + \rho_- = N/L$. Of the N particles, a fraction $\phi = N_+/N = \rho_+/\rho$ are of the type R while the remaining fraction $1-\phi$ are L particles. The corresponding fluxes are denoted by $J_\pm$. In both the limits $\phi = 1$ and $\phi = 0$ this model reduces to the ATM model [6, 7].

One unusual feature of this PRL model is that the flux does *not* vanish in the dense-packing limit $\rho \to 1$. In fact, in the full-filling limit $\rho = 1$, the *exact* non-vanishing flux $J_+ = K\rho_+\rho_- = J_-$ at $\rho_+ + \rho_- = \rho = 1$ arises only from the exchange of the R and L particles, irrespective of the magnitudes of f, Q and q.

In the special case $Q = q =: q_h$ the hopping of the ants become independent of pheromone. This special case of the PRL model is identical to the AHR model [39] with $q_- = 0 = \kappa$. A simple mean-field approximation yields the estimates

$$J_\pm \simeq \rho_\pm \left[q_h(1-\rho) + K c_\mp\right] \tag{12.22}$$

initial	final	rate
RL	RL	$1-K$
	LR	K
RP	RP	$(1-f)(1-Q)$
	R0	$f(1-Q)$
	0R	fQ
	PR	$(1-f)Q$
R0	R0	$1-q$
	0R	fq
	PR	$(1-f)q$

initial	final	rate
PR	PR	$1-f$
	0R	f
P0	P0	$1-f$
	00	f
PP	PP	$(1-f)^2$
	P0	$f(1-f)$
	0P	$f(1-f)$
	00	f^2

Fig. 12.14 Nontrivial transitions and their transition rates. Transitions from initial states PL, $0L$ and $0P$ are not listed. They can be obtained from those for LP, $L0$ and $P0$, respectively, by replacing $R \leftrightarrow L$ and, then, taking the mirror image

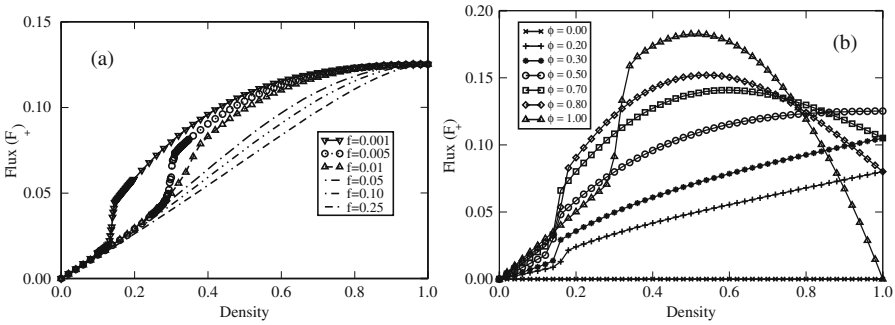

Fig. 12.15 The fundamental diagrams in the steady-state of the PRL model for several different values of (left) f (for $\phi = 0.5$) and (right) ϕ (for $f = 0.001$). The other common parameters are $Q = 0.75, q = 0.25, K = 0.5$ and $L = 1000$

irrespective of f, for the fluxes $J_\pm$ at any arbitrary ρ. These results agree reasonably well with the exact values of the flux [40] for all $q_h \geq 1/2$ but deviate more from the exact values for $q_h < 1/2$, indicating the presence of stronger correlations at smaller values of q_h.

For the generic case $q \neq Q$, the flux in the PRL model depends on the evaporation rate f of the P particles. Figure 12.15 shows fundamental diagrams for wide ranges of values of f (in Fig. 12.15a) and ϕ (in Fig. 12.15b). The data in Fig. 12.15 are consistent with the physically expected value of $J_\pm(\rho = 1) = K\rho_+\rho_-$, because in the dense packing limit only the exchange of the oppositely moving particles contributes to the flux. Moreover, the sharp rise of the flux over a narrow range of ρ observed in both Fig. 12.15a and b arise from the nonmonotonic variation of the average s peed with density observed in the unidirectional ATM [6, 7].

As we have seen earlier in Sect. 12.2.1, in the special limits $\phi = 0$ and $\phi = 1$, over a certain regime of density (especially at small f), the particles form loose (i.e., non-compact) clusters [7]. If the system evolves from a random initial condition at $t = 0$, then during coarsening of the cluster, its size $R(t)$ at time t is given by $R(t) \sim t^{1/2}$ [23, 24] see Fig. 12.16. Therefore, in the absence of encounter with oppositely moving particles, $\tau_\pm$, the coarsening time for the right-moving and left-moving particles would grow with system size as $\tau_+ \sim \phi^2 L^2$ and $\tau_- \sim (1-\phi)^2 L^2$.

In the PRL model with periodic boundary conditions, the oppositely moving loose clusters "collide" against each other periodically where the time gap τ_g between the successive collisions increases linearly with the system size ($\tau_g \sim L$). During a collision each loose cluster "shreds" the oppositely moving cluster; both clusters shred the other equally if $\phi = 1/2$ (Fig. 12.17a). However, for all $\phi \neq 1/2$, the minority cluster suffers more severe shredding than that suffered by the majority cluster (Fig. 12.17b) because each member of a cluster contributes in the shredding of the oppositely moving cluster. In small systems the "shredded" clusters get opportunity for significant re-coarsening before getting shredded again in the next encounter with the oppositely moving particles. But, in sufficiently large systems, shredded appearance of the clusters persists as demonstrated by the space-time plots for two different system sizes in Fig. 12.18.

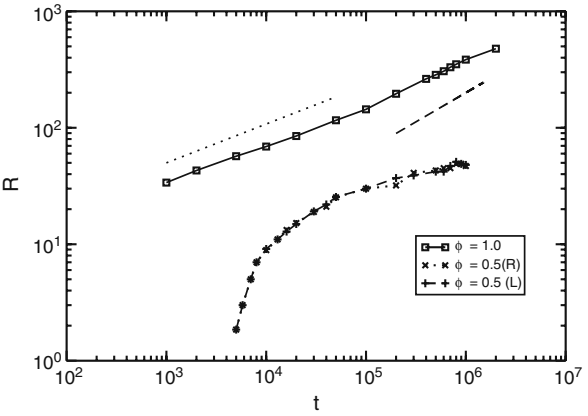

Fig. 12.16 Average size of the cluster R plotted against time t for $\phi = 1.0$, and $\phi = 0.5$, both for the same total density $\rho = 0.2$; the other common parameters being $Q = 0.75$, $q = 0.25$, $K = 0.50$, $f = 0.005$, $L = 4000$

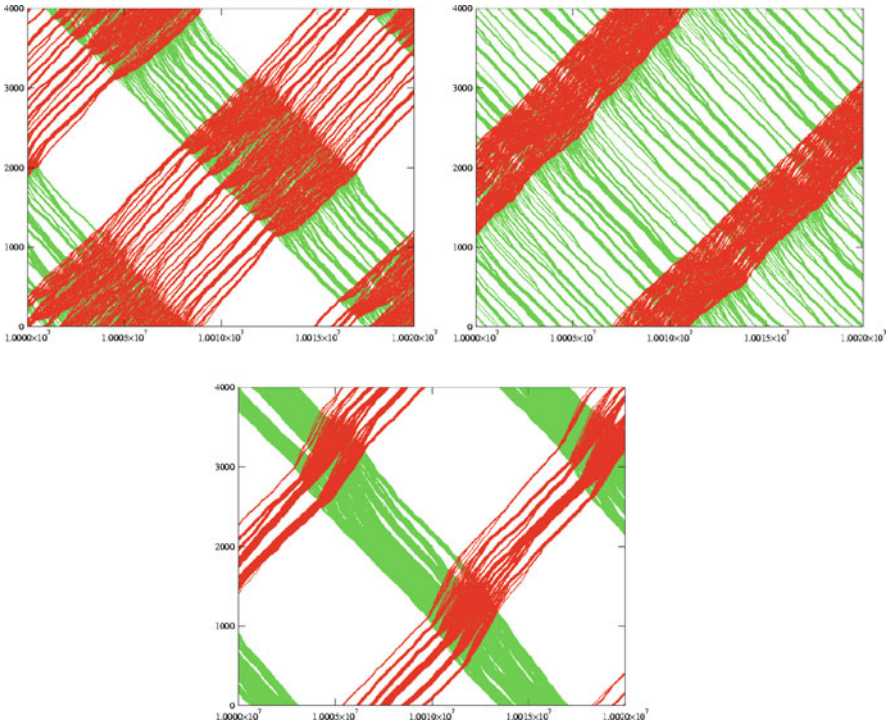

Fig. 12.17 Space-time plot of the PRL model for $Q = 0.75$, $q = 0.25$, $f = 0.005$, $L = 4000$, $\rho = 0.2$ and (a) $\phi = 0.5$, $K = 0.2$, (b) $\phi = 0.3$, $K = 0.2$, (c) $\phi = 0.3$, $K = 0.5$. The *red* and *green* dots represent the right-moving and left-moving ants, respectively

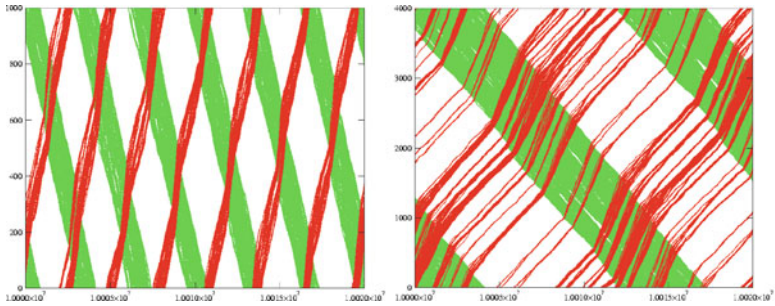

Fig. 12.18 Space-time plot of the PRL model for $Q = 0.50$, $q = 0.25$, $f = 0.005$, $\rho = 0.2$, $\phi = 0.3$, $K = 1.0$ and (**a**) $L = 1000$, (**b**) $L = 4000$. The *red* and *green dots* represent the right-moving and left-moving ants, respectively

Thus, coarsening and shredding phenomena compete against each other [37] and this competition determines the overall spatio-temporal pattern. Therefore, in the late stage of evolution, the system settles to a state where, because of alternate occurrence of shredding and coarsening, the typical size of the clusters varies periodically.

12.6 Empirical Results

The pioneering experiments on ant traffic [13] and all the subsequent related works [34, 38, 41–43] used bidirectional trails where the nature of flow is dominated by the head-on encounters of the ants coming from opposite directions [38, 34, 43]. But, in vehicular traffic, where flows in opposite directions are normally well separated and head-on collisions can occur only accidentally, the spatio-temporal organization of the vehicles in each direction is determined by the interactions of the vehicles moving in the same direction. Therefore, to allow for a better comparison between the two traffic systems, in [12] data from *unidirectional* traffic of ants on natural trails have been collected and analyzed using methods adapted from traffic engineering.

The experimental data were collected using video recordings of natural trails [44] where the natural situation was maintained focussing on sections of trails which had neither crossings nor branching and which remained unaltered for several hours. During the observation time the flow could be considered to be stationary and undisturbed by external factors. Data recorded at different trails of the same type basically revealed the same behaviour [44].

One of the distinct behavioral characteristics of individual ants observed in the course of recording is the absence of overtaking. Although some ants (temporarily) left the trail and were passed by succeeding ones, it was never observed any incident where an ant would speed up simply to overtake some other ant in front.

Since no overtaking takes place, ants can be uniquely identified by the ordered sequence in which they enter the observed section of the trail. Suppose, the nth ant enters the section at A at time $t_+(n)$ and leaves the section at B at time $t_-(n)$ (see Fig. 12.1). An efficient tool for analyzing such data is the *cumulative plot* (Fig. 12.19) [45]; it shows the numbers $n_+(t)$ and $n_-(t)$ of ants which have passed

the point A and B, respectively, up to time t. The two resulting curves, which are sometimes called *arrival function* and *departure function* can be obtained by inverting $t_+(n)$ and $t_-(n)$, respectively.

Using this strategy, the data could be analyzed very efficiently. The travel time $\Delta T(n)$ of the nth ant in the section between the points A and B is given by

$$\Delta T(n) = t_-(n) - t_+(n) \tag{12.23}$$

and the time-averaged speed of the nth ant during the period $\Delta T(n)$ is

$$v(n) = \frac{L}{\Delta T(n)} \tag{12.24}$$

The time-headway of two succeeding ants can be obtained easily at the entrance and exit points A and B (Fig. 12.19, left inset). Since $v(n)$ is, by definition (Eq. (12.24)), the time-averaged velocity $v(n)$ of the n-th ant, the distance-headway between the n-th ant and the ant in front of it is given by

$$\begin{aligned} \Delta d(n) &= \Delta t_+(n)\, v(n-1)\,, \\ \Delta t_+(n) &= t_+(n) - t_+(n-1)\,. \end{aligned} \tag{12.25}$$

Entry and exit of each ant changes the instantaneous number $N(t)$ of the ants in the trail section between A and B by one unit (Fig. 12.19, right inset). Therefore

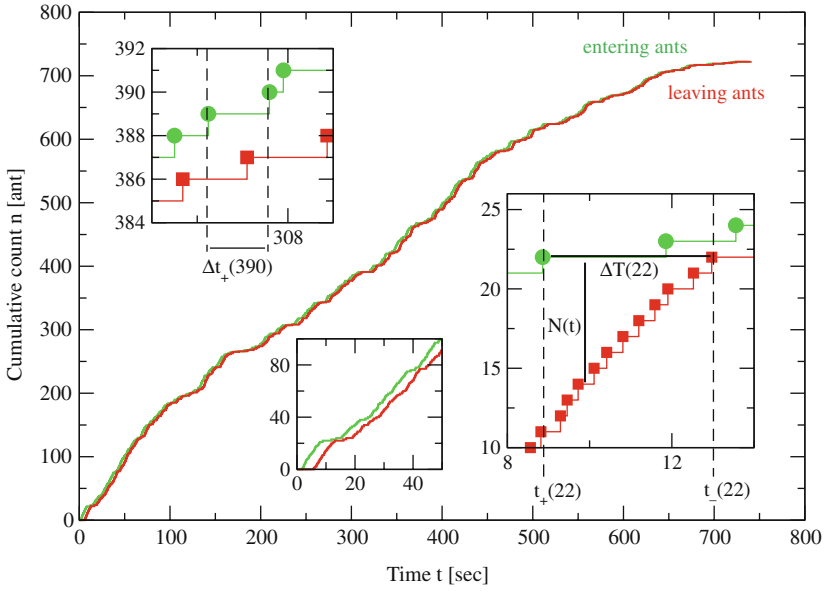

Fig. 12.19 Figure illustrating the technique employed for data extraction. The cumulative count of the ants which have entered $n_+(t)$ (•) and left $n_-(t)$ (□) the trail section between A and B. The *right inset* shows the travel time ΔT for the 22th ant. On the *left inset* the time-headway Δt_+ of the 390th ant is shown

$N(t)$ fluctuates, but stays constant in between two events of entry or exit. Sorting the counts of these events by time one obtains a chronological list $\{t_i\} = \{t_\pm(n)\}$ of the changes of the instantaneous particle number

$$N(t) = n_+(t) - n_-(t) = const. \quad \text{while } t \in [t_i, t_{i+1}[. \tag{12.26}$$

Next we estimate the effective local density experienced by the n-th ant at a given instant of time. During the time interval $\Delta T(n)$ it spends within the observed trail section, the average number of ants in the same section is given by

$$\langle N \rangle_{t(n)} = \frac{1}{\Delta T(n)} \sum_{t_i = t_+(n)}^{t_i < t_-(n)} N(t_i)(t_{i+1} - t_i) \tag{12.27}$$

During the same time interval, the (dimensionless) density $\rho(n)$ affecting the movement of the n-th ant is given by

$$\rho(n) = \frac{\langle N \rangle_{t(n)}}{N_{\max}} = \frac{\tilde{\rho}(n)}{\tilde{\rho}_{\max}} \qquad \text{with} \quad \tilde{\rho}(n) = \frac{\langle N \rangle_{t(n)}}{L}\,, \tag{12.28}$$

where $N_{\max} = 17 = L/(1\text{ bl})$ and $\tilde{\rho}_{\max} = N_{\max}/L$; bl being the body length of an ant ($1bl \approx 18$ mm). The instantaneous particle numbers and the single-ant velocity are averaged over the same time-interval $\Delta T(n)$.

Figure 12.20 shows the fundamental diagram obtained from this analysis. The most unusual feature is that, unlike vehicular traffic, there is no significant decrease of the average velocity with increasing density. Consequently, the flux increases approximately linearly over the entire regime $\rho \in [0, 0.8]$ of observed density. The jammed branch of the fundamental diagram, which is commonly observed in vehicular traffic and which is characterized by a monotonic decrease of flow with increas-

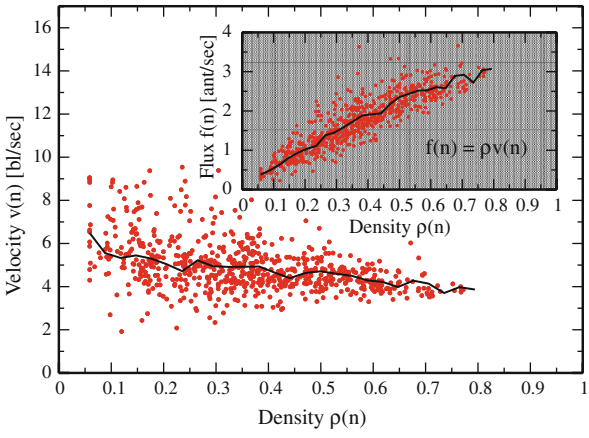

Fig. 12.20 Average velocity (*solid line*) and single-ant velocities (*dots*) for unidirectional single-lane trail section of length $L = 17$ bl. The corresponding flux-velocity relation is plotted in the inset. Mutual blocking is obviously suppressed as the average velocity is almost independent of the density. Consequently, the flux increases almost linearly with the density in the fundamental diagram (see *inset*)

ing density, is completely missing. Obviously effects of mutual blocking, which are normally expected to become dominant at high densities are strongly suppressed in ant traffic.

From the time-series of the single-ant velocities also their distributions in different density regimes can be determined. The most striking feature is that it becomes much sharper with increasing global density whereas the most probable velocity decreases only slighty [12].

Another important quantity that characterizes the spatial distribution of the ants on the trail is the distance-headway distribution [12]. Time-series show clustering of small distance-headways whereas larger headways are much more scattered. The distribution of these headways becomes much sharper with increasing density while the maximum shifts only slightly to smaller headways. At low densities, predominantly large distance-headways are found; the corresponding distribution for sufficiently long distance-headways is well described by a negative-exponential distribution which is characteristic of the so-called random-headway state [46]. In contrast, at very high densities mostly very short distance-headways are found; in this regime, the log-normal distribution appears to provide the best fit to the empirical data.

The absence of a jammed phase in the fundamental diagram is closely related to the characteristic features of the distributions of the distance-headways of the ants along the observed section of the trail. The dominant, and directly observable, feature of this spatial distribution is the platoons formed by the ants, as predicted by the models discussed before. Ants inside a platoon move with almost identical velocities maintaining small distance-headways. These intra-platoon distance-headways are responsible for the clustering of data observed in the corresponding time-series [12]. In contrast, larger distance-headways are inter-platoon separations. The full distribution of distance-headways has an average of $D = 2.59$ bl which is quite close to the value $D = 1.66$ bl found for very high densities. This indicates the existence of a density-independent distance-headway for the ants moving inside platoons.

The interpretations of the observed trends of variations of the flux, average velocity and distance-headway distribution with increasing density is consistent with the corresponding variation of the distribution of the velocities of the ants. Ants within a platoon move at a slower average velocity whereas solitary ants can move faster if they detect a strong pheromone trace created by a preceeding platoon. Moreover, since fluctuations of velocities of different platoons are larger than the intra-platoon fluctuations, the distribution becomes sharper at higher densities because the platoons merge thereby reducing their number and increasing the length of the longest one. The maximum of the velocity distribution is almost independent of the density. Its position at sufficiently large densities can be interpreted as platoon velocity, $v_p \approx 4.6$ bl/s.

It is worth pointing out that physical origin of the occurrence of the nearly constant average velocity of the vehicles in highway traffic is very different from the constant velocity of ants in ant traffic. In vehicular traffic, the average velocity of the vehicles remains practically unaffected by increasing density, provided the density is sufficiently low, because at those densities the vehicles are well separated from each other and, therefore, can move practically unhindered in the so-called free-flow

state. On the other hand, in ant traffic, this constant velocity regime is a reflection of the fact that ants march together collectively forming platoons which reduce the effective density.

Thus, in spite of some superficial similarities, the characteristic features of ant traffic seem to be rather different from those of vehicular traffic. Perhaps, ant traffic is analogous to human pedestrian traffic [47, 42, 43], as was conjectured beautifully by Hölldobler and Wilson in their classic book [10].

12.7 Concluding Discussions

Several theoretical investigations have been carried out earlier, in terms of CA, to study the emergence of the trail patterns in ant colonies [4]. However, to our knowledge, our work is the first attempt to understand the traffic-like flow of ants on well formed trails using the language of CA. Here we have reviewed, in some detail, the stochastic cellular automaton model of an ant trail introduced in [6] and some of its generalizations. The model is characterized by two coupled dynamical variables, representing the ants and the pheromone. Under periodic boundary conditions, one of the variables (ants) is conserved, whereas the other variable (pheromone) is always a non-conserved variable. The dynamics of these two variables are coupled to each other. This coupling leads to surprising results, especially an anomalous fundamental diagram which arises from an unusual non-monotonic variation of the average speed of the ants with their density on the trail in the intermediate regime of the ant density. We would like to emphasize that this surprising result could not be anticipated as a trivial consequence of the dynamical prescriptions of the model. It is only over a range of pheromone-evaporation rate that the surprising increase of average velocity of ants with increasing density was observed.

Our experimental investigations on real ant trails have, indeed, exposed some unusual features of the fundamental diagram. The average velocity is practically independent of density. This, in turn, leads to the complete absence of a jammed branch in the fundamental diagram. In order to test the possibility of the non-monotonic variation of the average velocity with density, our experiment should be repeated with a circular trail which would mimic the trail under period boundary conditions. Our first set of experiments have already unveiled a totally unexpected feature of the fundamental diagram of the ant trafic. Clearly there is a need for extension of our model to account for the observed features of the fundamental diagram. At present we are actively considering several possible realistic extensions of our model. These include (a) different levels of concentration of pheromone at each site, (b) diffusional spread of pheromone, (iii) tendency of persistent movement of ants, etc.

Acknowledgements We thank our collaborators V. Guttal, A. Kunwar, K. Sugawara, T. Kazama and especially Alexander John for many discussions. Research of the group of one of the authors (DC) is supported by CSIR (India). DC also thanks Alexander von Humboldt Foundation for re-invitation, under the Humboldt Alumni program, to the university of Köln where part of this work was completed.

References

1. S. Wolfram, *Theory and Applications of Cellular Automata* (World Scientific, Singapore, 1986)
2. B. Chopard, M. Droz, *Cellular Automata Modelling of Physical Systems* (Cambridge University Press, 1998)
3. D. Chowdhury, L. Santen, A. Schadschneider, Statistical physics of vehicular traffic and some related systems. Phys. Rep. **329**, 199–329 (2000)
4. D. Chowdhury, K. Nishinari, A. Schadschneider, Self-organized patterns and traffic flow in colonies of organisms: From bacteria and social insects to vertebrates. Phase Transit. **77**, 601–624 (2004)
5. D. Chowdhury, K. Nishinari, A. Schadschneider, Physics of transport and traffic phenomena in biology: From molecular motors and cells to organisms. Phys. Life Rev. **2**, 318 (2005)
6. D. Chowdhury, V. Guttal, K. Nishinari, A. Schadschneider, A cellular-automata model of flow in ant trails: Non-monotonic variation of speed with density. J. Phys. A: Math. Gen. **35**, L573–L577 (2002)
7. K. Nishinari, D. Chowdhury, A. Schadschneider, Cluster formation and anomalous fundamental diagram in an ant trail model. Phys. Rev. E **67**, 036120 (2003)
8. D. Helbing, Traffic and related self-driven many-particle systems. Rev. Mod. Phys. **73**, 1067 (2001)
9. B. Kerner: *The Physics of Traffic* (Springer, Heidelberg, 2004)
10. B. Hölldobler, E.O. Wilson, *The Ants* (Belknap, Cambridge, 1990)
11. B. Hölldobler, E.O. Wilson: *The Superorganism: The Beauty, Elegance, and Strangeness of Insect Societies* (W.W. Norton, New York, 2008)
12. A. John, A. Schadschneider, D. Chowdhury, K. Nishinari, Trafficlike collective movement of ants on trails: Absence of jammed phase. Phys. Rev. Lett. **102**, 108001 (2009)
13. M. Burd, D. Archer, N. Aranwela, D.J. Stradling, Traffic dynamics of the leaf cutting ant. American Natur. **159**, 283 (2002)
14. F. Schweitzer, *Brownian Agents and Active Particles*, Springer Series in Synergetics (Springer, Heidelberg, 2003)
15. S. Camazine, J.L. Deneubourg, N.R. Franks, J. Sneyd, G. Theraulaz, E. Bonabeau, *Self-organization in Biological Systems* (Princeton University Press, Princeton, 2001)
16. A.S. Mikhailov, V. Calenbuhr, *From Cells to Societies* (Springer, Berlin, 2002)
17. B. Derrida, An exactly soluble non-equilibrium system: The asymmetric simple exclusion process. Phys. Rep. **301**, 65 (1998)
18. B. Derrida, M.R. Evans, in: *Nonequilibrium Statistical Mechanics in One Dimension*, ed. by V. Privman (Cambridge University Press, Cambridge, 1997)
19. G.M. Schütz, Exactly solvable models for many-body systems far from equilibrium, ed. by C. Domb, J.L. Lebowitz, *Phase Transitions and Critical Phenomena*, Vol. 19, (Academic Press, London, UK, 2000)
20. R.A. Blythe, M.R. Evans, Nonequilibrium steady states of matrix product form: a solver's guide. J. Phys. A **40**, R333 (2007)
21. A. Kunwar, A. John, K. Nishinari, A. Schadschneider, D. Chowdhury, Collective traffic-like movement of ants on a trail – dynamical phases and phase transitions. J. Phys. Soc. Jpn. **73**, 2979 (2004)
22. K. Nishinari, D. Takahashi, Analytical properties of ultradiscrete Burgers equation and rule-184 cellular automaton. J. Phys. A: Math. Gen. **31**, 5439 (1998)
23. O.J. O'Loan, M.R. Evans, M.E. Cates, Jamming transition in a homogeneous one-dimensional system: The bus route model. Phys. Rev. E **58**, 1404 (1998)
24. D. Chowdhury, R.C. Desai, Steady-states and kinetics of ordering in bus-route models: Connection with the Nagel-Schreckenberg model. Eur. Phys. J. B **15**, 375 (2000)
25. F. Spitzer, Interaction of Markov processes. Adv. Math. **5**, 246–290 (1970)
26. M.R. Evans, Phase transitions in one-dimensional nonequilibrium systems. Braz. J. Phys. **30**, 42 (2000)

27. M.R. Evans, T. Hanney, Nonequilibrium statistical mechanics of the zero-range process and related models. J. Phys. A **38**, R195 (2005)
28. M.R. Evans, Exact steady states of disordered hopping particle models with parallel and ordered sequential dynamics. J. Phys. A **30**, 5669 (1997)
29. A.B. Kolomeisky, G. Schütz, E.B. Kolomeisky, J.P. Straley, Phase diagram of one-dimensional driven lattice gases with open boundaries. J. Phys. A **31**, 6911 (1998)
30. V. Popkov, G. Schütz, Steady-state selection in driven diffusive systems with open boundaries. Europhys. Lett. **48**, 257 (1999)
31. K. Nishinari, K. Sugawara, T. Kazama, A. Schadschneider, D. Chowdhury, Modelling of self-driven particles: Foraging ants and pedestrians. Physica A **372**, 132 (2006)
32. A. John, A. Schadschneider, D. Chowdhury, K. Nishinari, Collective effects in traffic on bi-directional ant trails. J. Theor. Biol. **231**, 279 (2004)
33. R. Beckers, J.L. Deneubourg, S. Goss, Trails and U-turns in the selection of a path by the ant *Lasius niger*. J. Theor. Biol. **159**, 397 (1992)
34. I.D. Couzin, N.R. Franks, Self-organized lane formation and optimized traffic flow in army ants. Proc. Roy Soc. London B **270**, 139 (2003)
35. S.A. Janowsky, J.L. Lebowitz, Finite-size effects and shock fluctuations in the asymmetric simple-exclusion process. Phys. Rev. A **45**, 618 (1992)
36. G. Tripathy, M. Barma, Steady state and dynamics of driven diffusive systems with quenched disorder. Phys. Rev. Lett. **78**, 3039 (1997)
37. A. Kunwar, D. Chowdhury, A. Schadschneider, K. Nishinari, Competition of coarsening and shredding of clusters in a driven diffusive lattice gas. J. Stat. Mech. (2006) P06012
38. M. Burd, N. Aranwela, Head-on encounter rates and walking speed of foragers in leaf-cutting ant traffic. Insect. Sociaux **50**, 3 (2003)
39. P. F. Arndt, T. Heinzel, V. Rittenberg, Spontaneous breaking of translational invariance in one-dimensional stationary states on a ring. J. Phys. A **31**, L45 (1998); J. Stat. Phys. **97**, 1 (1999)
40. N. Rajewsky, T. Sasamoto, E.R. Speer, Spatial particle condensation for an exclusion process on a ring. Physica A **279**, 123 (2000)
41. K. Johnson, L.F. Rossi, A mathematical and experimental study of ant foraging trail dynamics. J. Theor. Biol. **241**, 360 (2006)
42. A. Dussutour, J.L. Deneubourg, V. Fourcassié, Temporal organization of bi-directional traffic in the ant Lasius niger (L.), Jrl. Exp. Biol. **208**, 2903 (2005)
43. A. John, A. Schadschneider, D. Chowdhury, K. Nishinari, Characteristics of ant-inspired traffic flow – Applying the social insect metaphor to traffic models. Swarm Intelligence **3**, 199 (2008)
44. A. John, *Physics of Traffic on Ant Trails and Related Systems*, Doctoral Thesis, (Universität zu Köln, Cologne, Germany, 2006)
45. P. Chakroborty, A. Das, *Principles of Transportation Engineering* (Prentice Hall of India, Englewood Cliffs, NJ, 2003)
46. A.D. May, *Traffic Flow Fundamentals* (Prentice Hall Englewood Cliffs, NJ, 1990)
47. C. Burstedde, K. Klauck, A. Schadschneider, J. Zittartz, Simulation of pedestrian dynamics using a 2-dimensional cellular automaton. Physica A **295**, 507 (2001)